
李政道研究所
Tsung-Dao Lee Institute

# Latent Generative Model for Calorimeter Fast Simulation

**Qibin LIU**, Chase Shimmin,
Xiulong LIU, Eli Shlizerman,
Shih-Chieh HSU, Shu LI

# Introduction

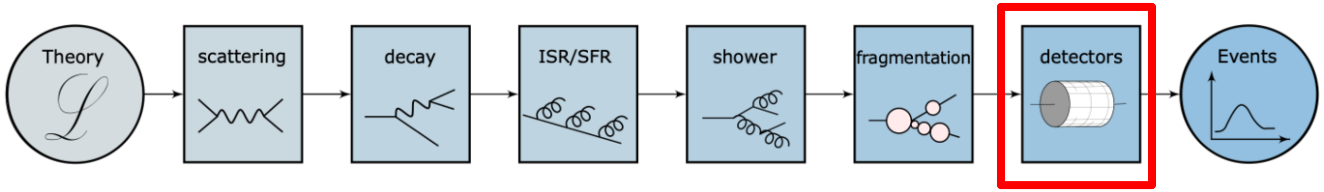


Machine Learning and LHC Event Generation, A. Butter et al. [2203.07460]

- Important step in the HEP workflow: Detector Simulation
- Calorimeter: "largest" part both in scale and computing cost
- Fast Simulation: most wanted and mandatory in the future
- Ultra-fast and scalable solution: latent generative model
- Implementations on CaloChallenge2022 datasets

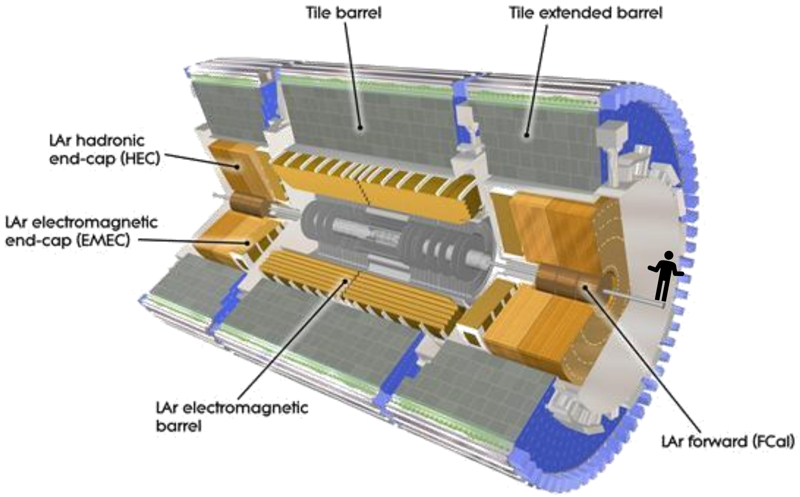


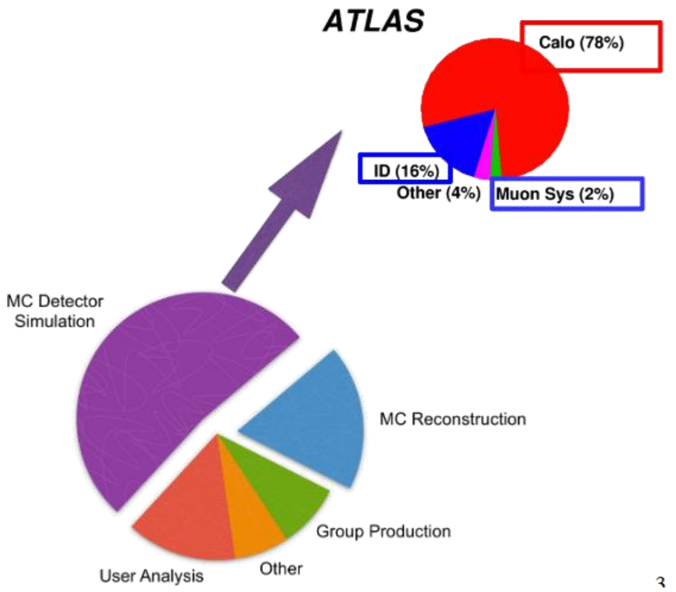


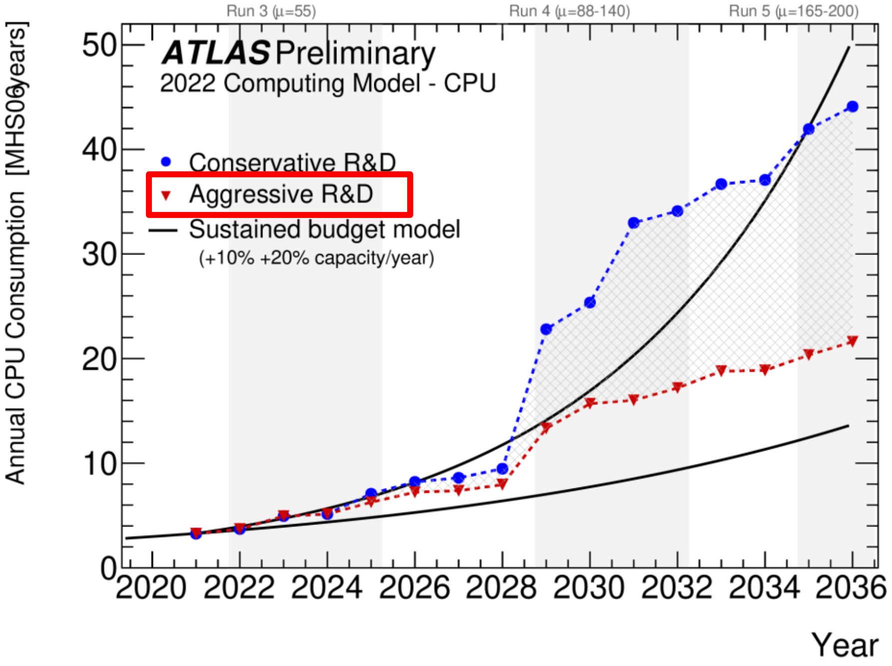


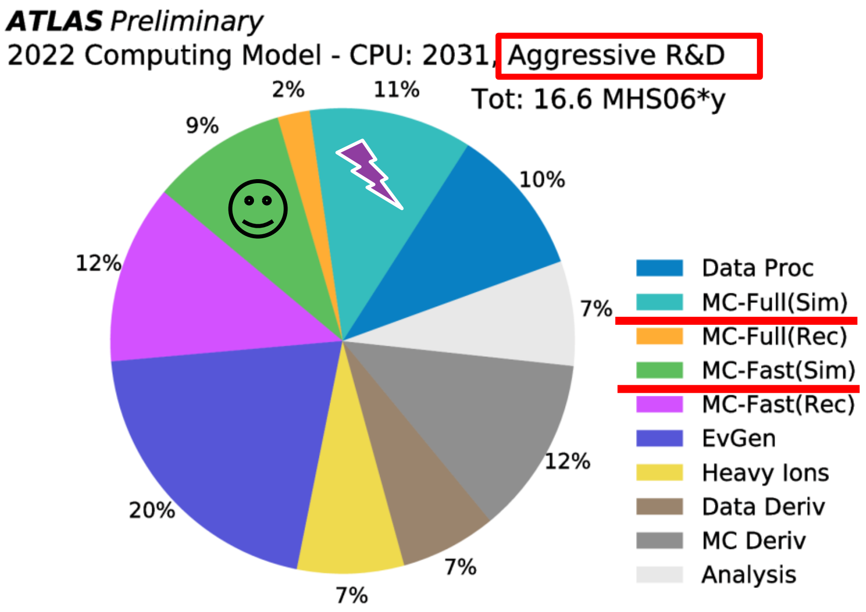


CERN-LHCC-2022-005

# Introduction

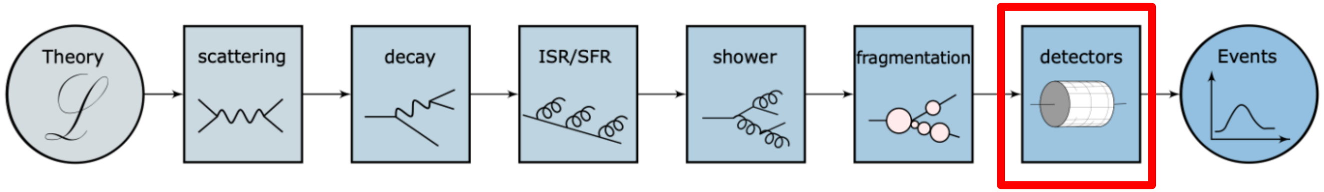


Machine Learning and LHC Event Generation, A. Butter et al. [2203.07460]

- Important step in the HEP workflow: Detector Simulation
- Calorimeter: "largest" part both in scale and computing cost
- Fast Simulation: most wanted and mandatory in the future
- Ultra-fast and scalable solution: latent generative model
- Implementations on CaloChallenge2022 datasets

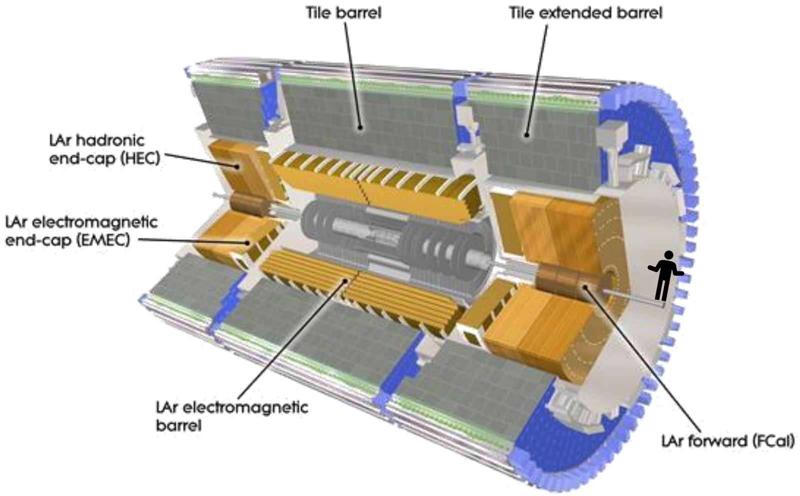


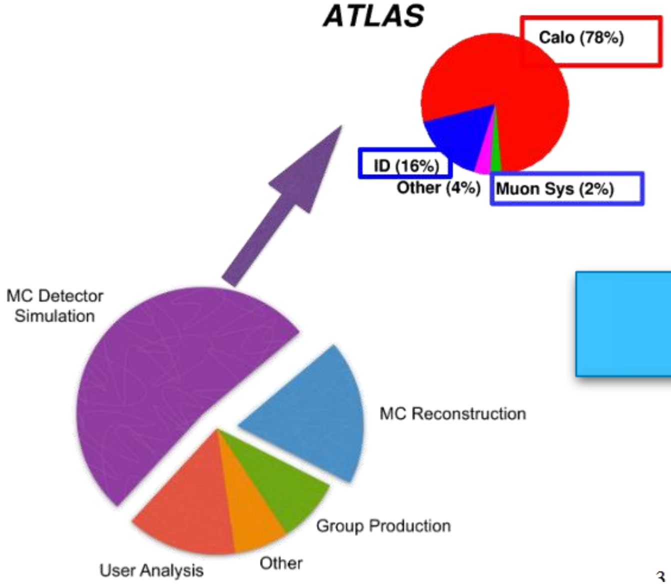


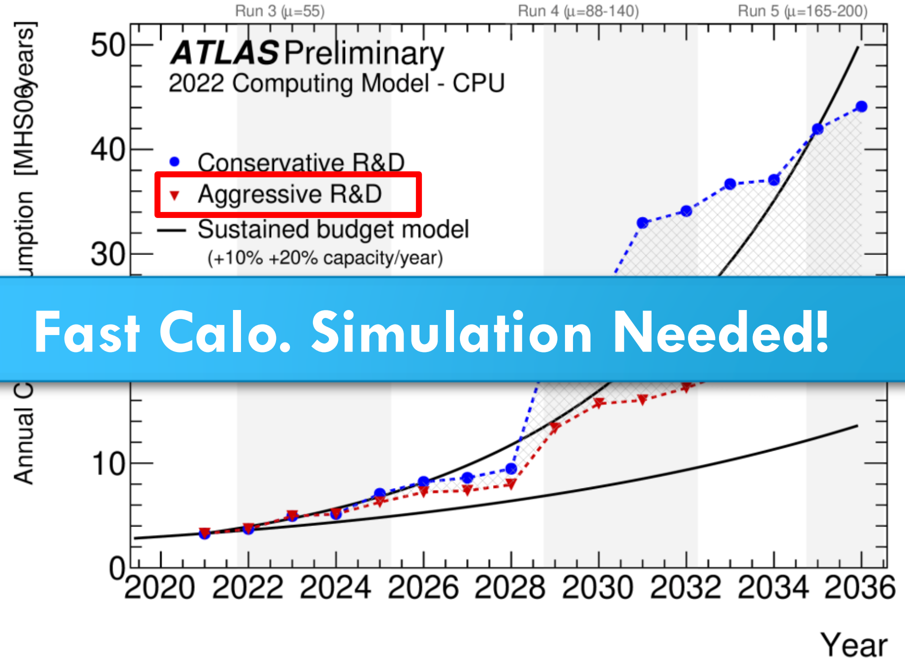


Fast Calo. Simulation Needed!

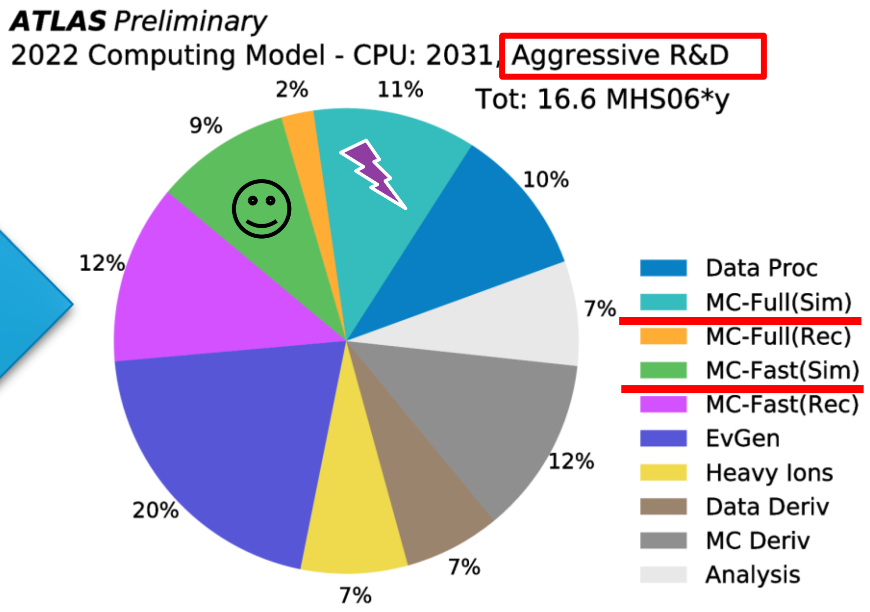


CERN-LHCC-2022-005

# Simulation of Calorimeter

- Simulate hits $\vec{E}$ corresponding to each calo. readout channel
- Full simulation(GEANT4): Tracing of every secondary particle
- Fast simulation: generate response in one/few pass(es)
- **VAE- based generative model: fast and well-controlled latent space**

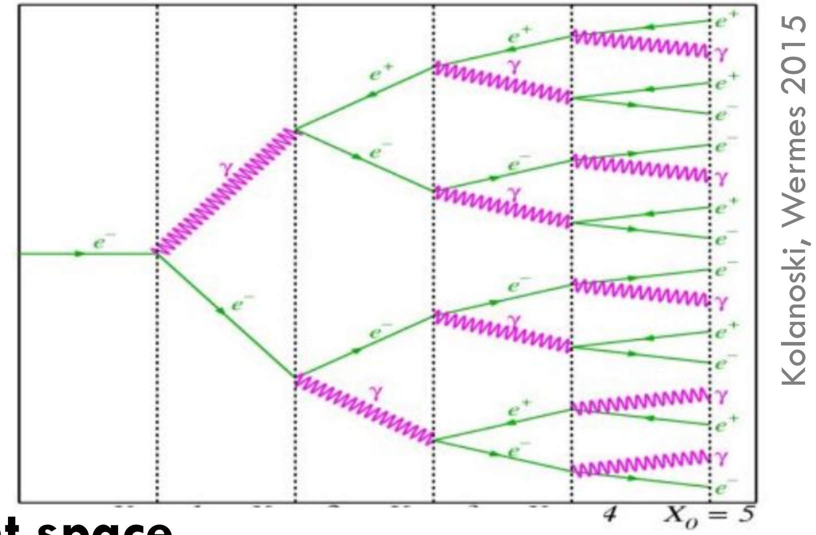


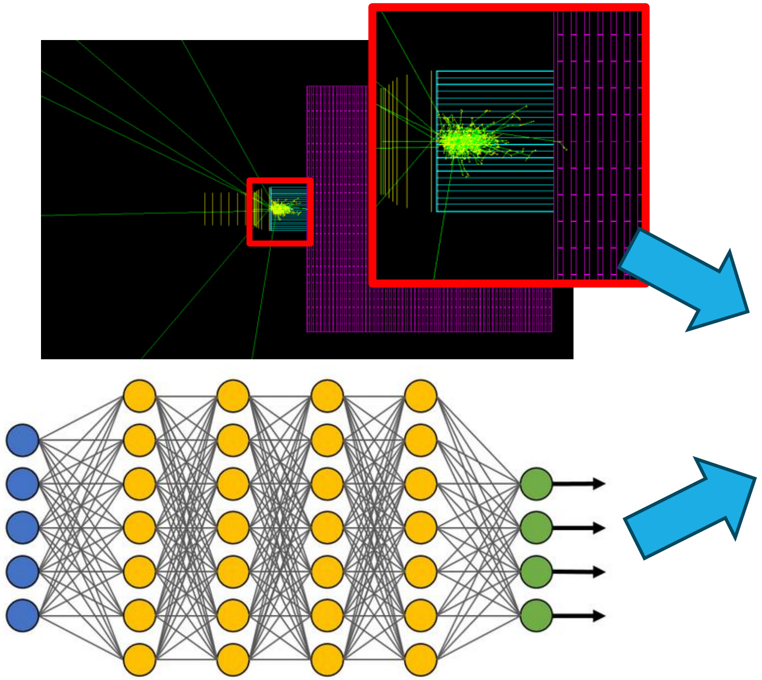

$$P(\overrightarrow{E_i}|E_{inc}, type, ..)$$

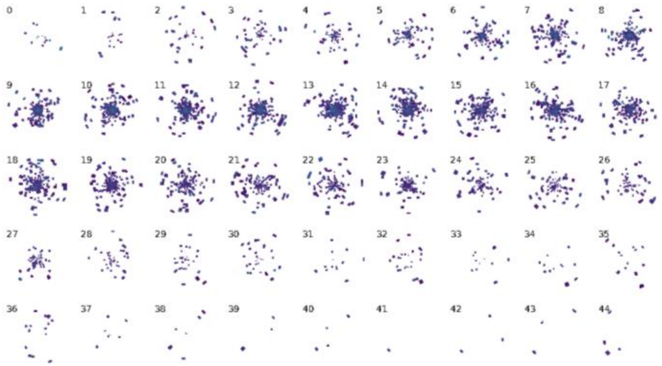

1 Shower on 45 layers calo.

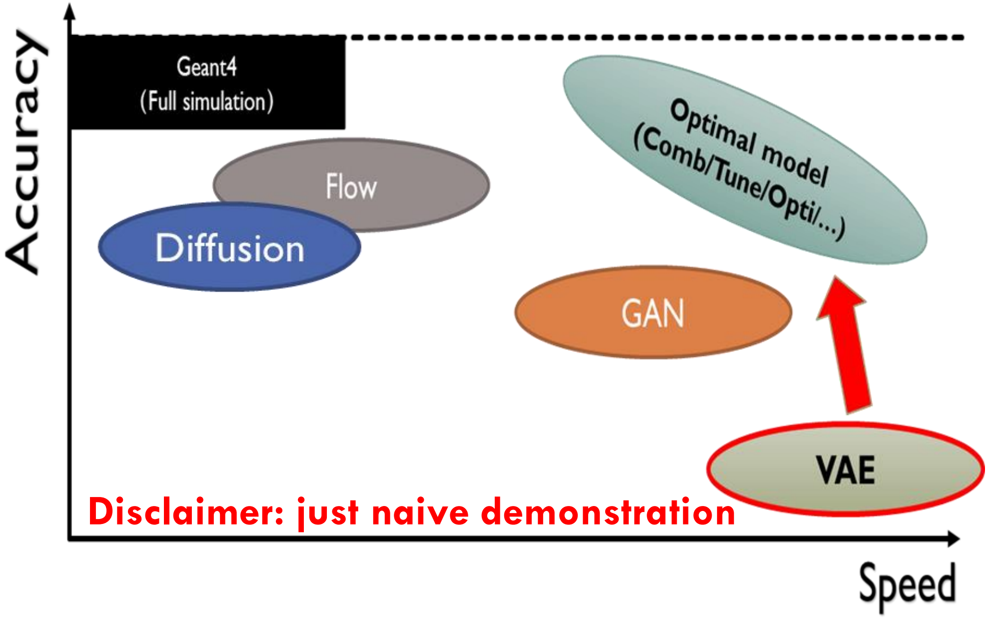

# Two-Step Generative Model: *Encoding*

Step1

- Compress and encode the calo. data into latent space: **"Auto-Encoder"**
- Quantized the latent space into code with **Vector Quantization** [1711.00937]
- $\mathbb{R}^D \rightarrow \mathbb{Z}^L$: Large compression ratio ($D \gg L$) and more descriptive
- Well defined objective and good scaling in general

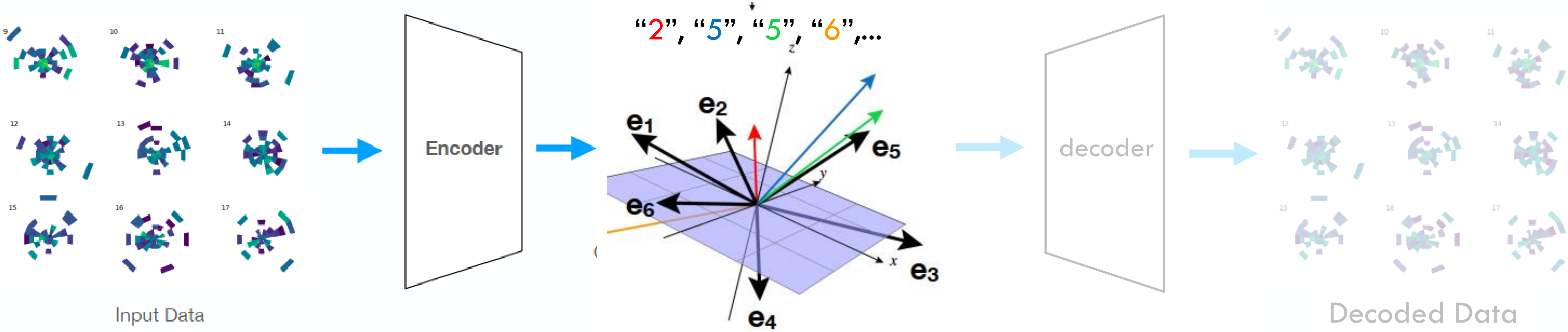


$$\left\| \mathrm{sg}[z_{enc}(x)] - e \right\|^2 + \beta \left\| z_{enc}(x) - \mathrm{sg}[e] \right\|^2$$

**Vector Quantization**
Dictionary learning // Update codebook

**Commitment Loss**
Tries to keep encoder predictions close to codebook values.

# Two-Step Generative Model: *Sampling*

*Step2*

➢Latent (codes) sampled with token model: RNN/PixelCNN/Transformer...

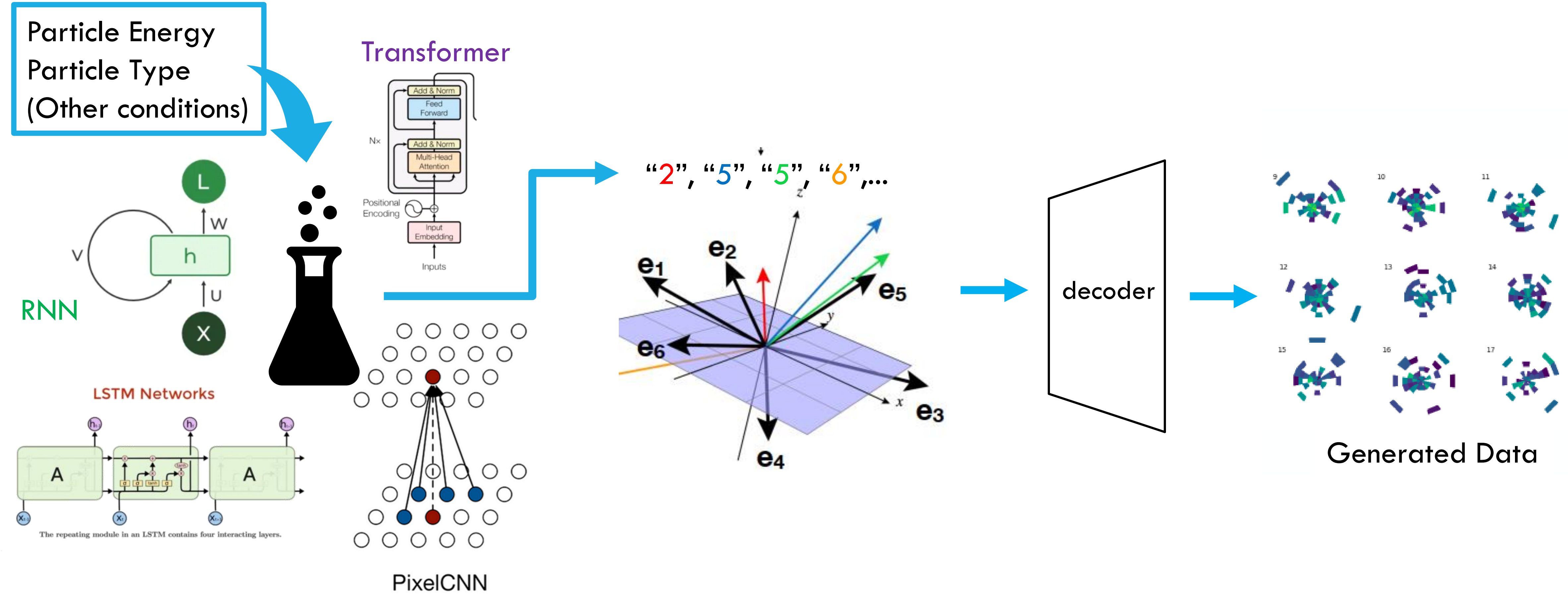


ML4JETS2023

Figures sources: aishwarya.27, 1706.03762, Colah, 1601.06759

# Two-Step Generative Model: *Sampling*

*Step2*

- Latent (codes) sampled with token model: RNN/PixelCNN/Transformer...
- **Bridge to modern rapidly developed AI model: GPT (imp. minGPT)**

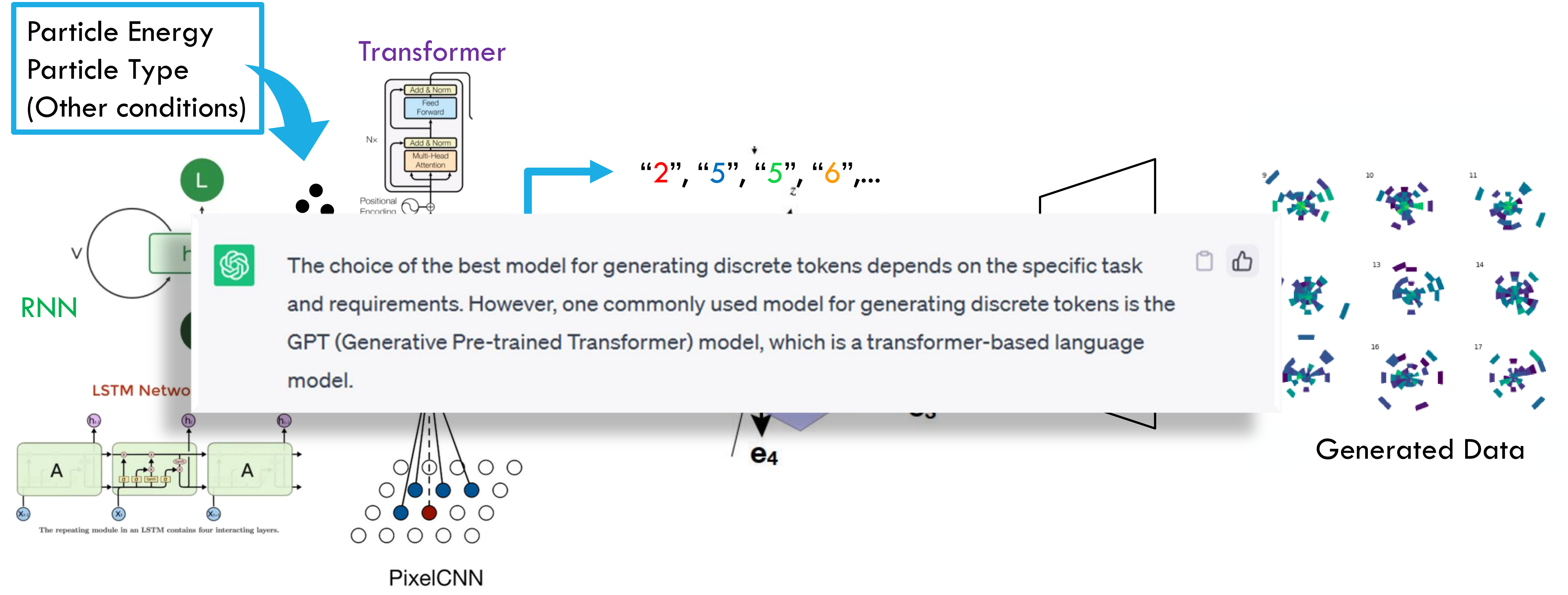


ML4JETS2023

Figures sources: aishwarya.27, 1706.03762, Colah, 1601.06759

# Dataset and Preprocessing

- ➢ Common calo. dataset: [CaloChallenge2022]
  - ❑ Cylinder with 384~40500 channels
  - ❑ Particle incident energy $E_c$: GeV ~ TeV $(\gamma, \pi, e)$
  - ❑ Large dynamic range: KeV ~ GeV for each channel $E_i$
  - ❑ High sparsity: most channels empty and compressible
- ➢ Preprocessing: Normalization & *Log* ⟺ SoftMax & *Exp*

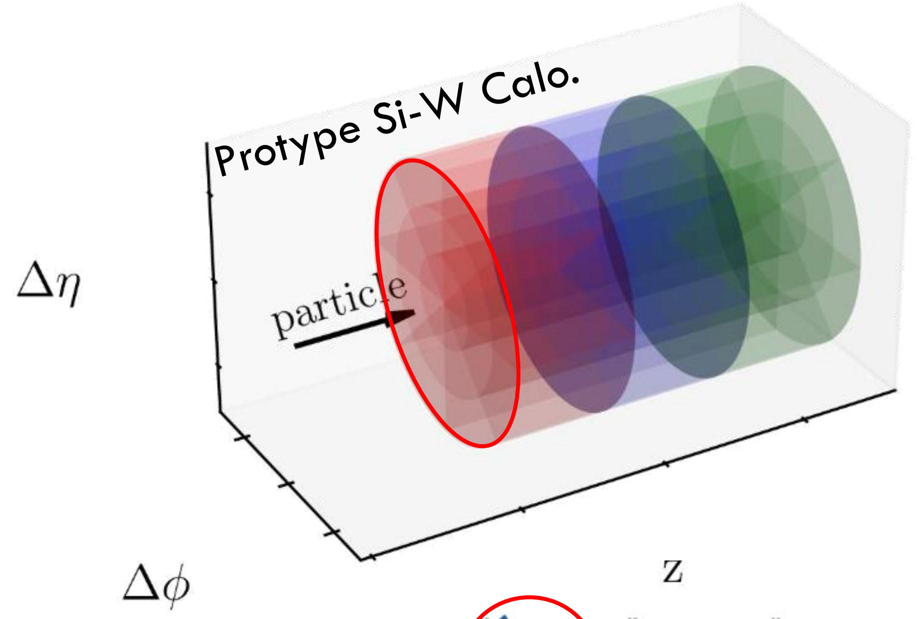


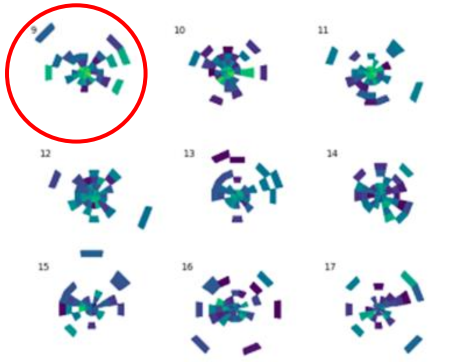

$$\sigma(\mathbf{z})_i = \frac{e^{z_i}}{\sum_{j=1}^{K} e^{z_j}}$$

$E_c$=20[GeV]

| | | |
|---|---|---|
| 1 | 2 | 1 |
| 1 | 8 | 2 |
| 1 | 1 | 1 |

$\sum E_i$ =18[GeV]

Normalized by $\sum E_i$

| | | |
|---|---|---|
| 0.06 | 0.11 | 0.06 |
| 0.06 | 0.44 | 0.11 |
| 0.06 | 0.06 | 0.06 |

R≡$\sum E_i / E_c$=0.9

Logarithm +Scaling

| | | |
|---|---|---|
| 0.56 | 0.63 | 0.56 |
| 0.56 | 0.78 | 0.63 |
| 0.56 | 0.56 | 0.56 |

Encoder Pass

Soft-max Output

| | | |
|---|---|---|
| -1.26 | -1.26 | -1.26 |
| -1.26 | -0.41 | -0.78 |
| -1.26 | -0.95 | -1.26 |

Decoder Pass

Exponential

| | | |
|---|---|---|
| 0.06 | 0.06 | 0.06 |
| 0.06 | 0.39 | 0.17 |
| 0.06 | 0.11 | 0.06 |

Recover by $\sum E_i$

| | | |
|---|---|---|
| 1 | 1 | 1 |
| 1 | 7 | 3 |
| 1 | 2 | 1 |

$\sum E_i$=R*$E_c$=18[GeV]

Sampled by Latent Model

# Step1 Implementation: VQGAN

$$Q^* = \arg\min_{E,G,\mathcal{Z}} \max_{D} \mathbb{E}_{x\sim p(x)} \Big[\mathcal{L}_{\mathrm{VQ}}(E,G,\mathcal{Z}) + \lambda \mathcal{L}_{\mathrm{GAN}}(\{E,G,\mathcal{Z}\},D)\Big]$$

- VQVAE combined with adversary trained discriminator (VQGAN)
  - Pixel-wise loss: L2 (MSE) loss comparing input and decoded $\|\boldsymbol{E}' - \boldsymbol{E}\|^2$
  - Physics-aware loss: shower center and width difference,... $|\boldsymbol{\eta} \cdot (\boldsymbol{E}' - \boldsymbol{E})|$

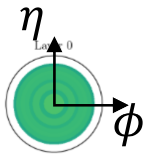


- Shower information compressed into latent space as *codes*

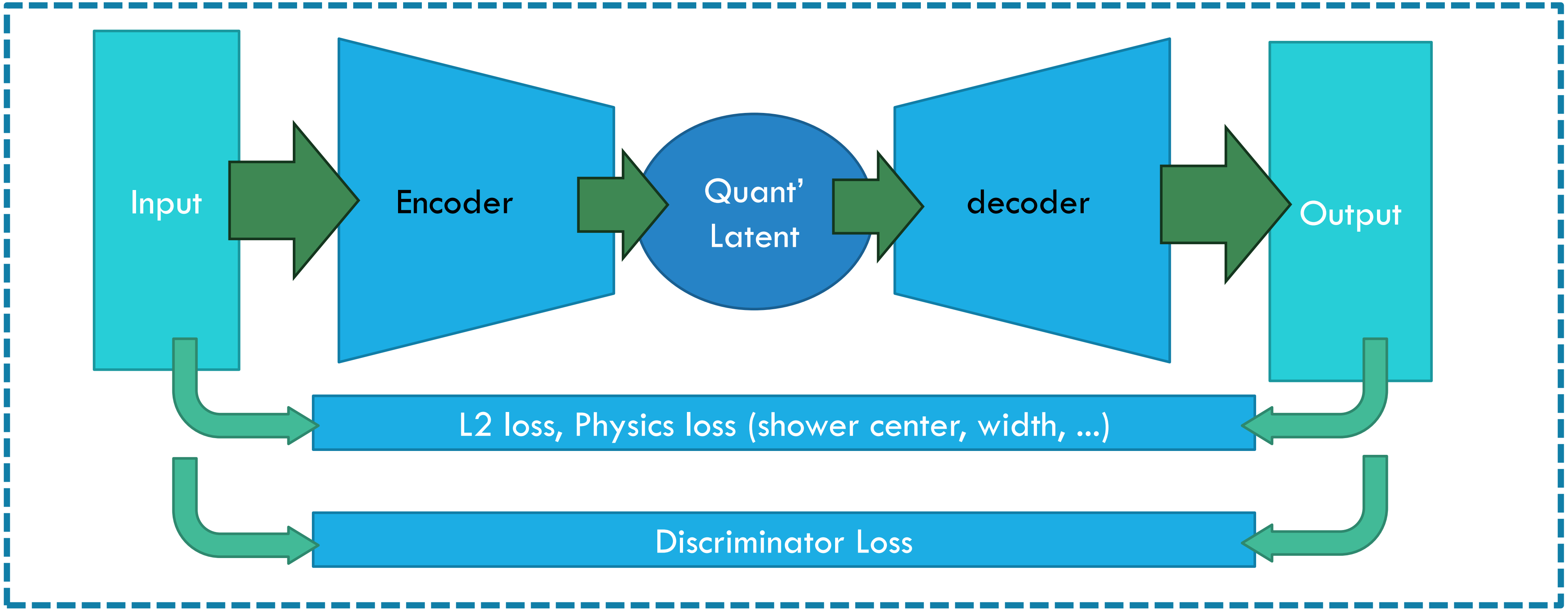

# Step2 Implementation: "Shower Language"

➢Physical information embedded in the discrete tokens:

❑Total energy response R ( $\sum E_i/E_c$) encoded with **digitization**

❑Shower information ($E_i/\sum E_i$) from Step1 output codes

➢**General for any specific calo. geometry, datasets, …**

➢Sampled with token model: e.g. transformer

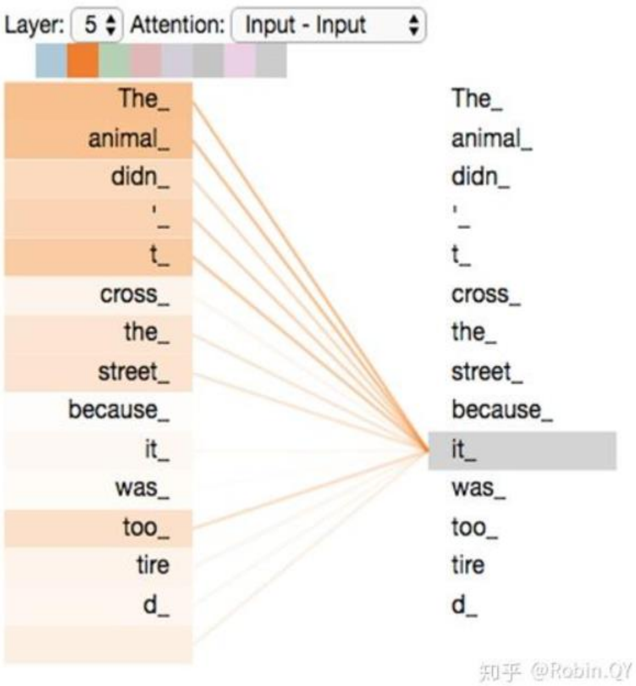


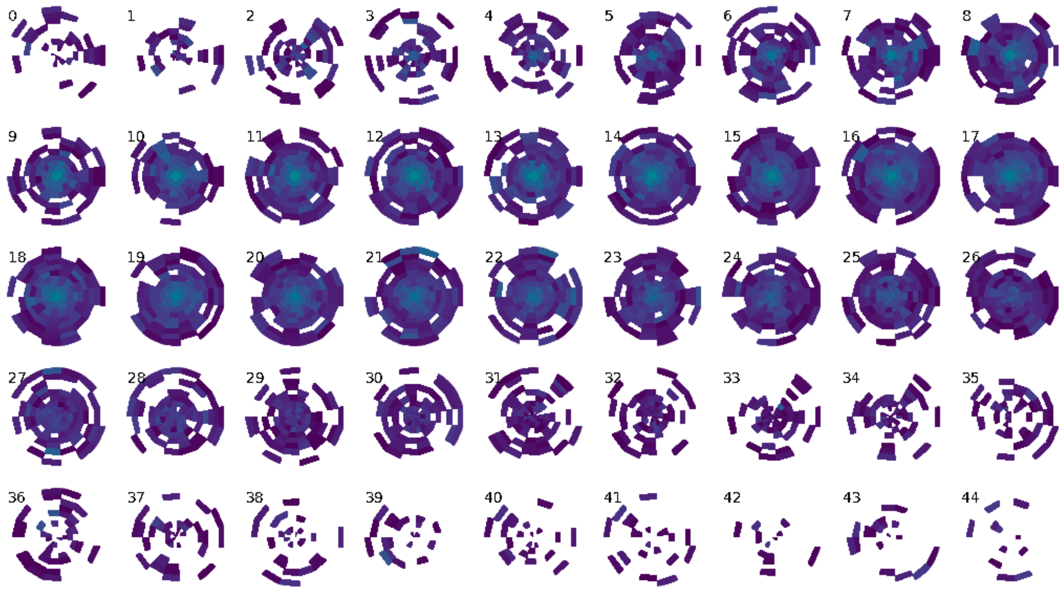


Calo. Data

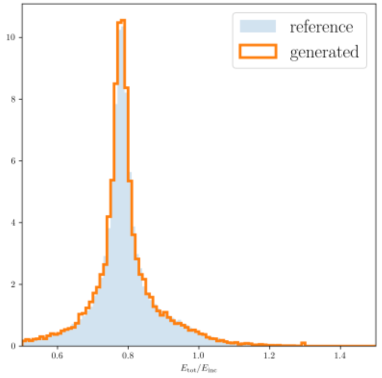


Language token

Digitized R

Shower symbols(codes)

09000⌂♋•♎♍❖↗♑♒♒♌…

"Shower Language"

# Performance on Small Dataset($\pi$)

- Small and irregular geometry: fully connected layers utilized
- Average shower: matches ground truth for all calo. layers
- Energy response: good agreement in wide energy range
- Dist. of physics variables: $\langle S^2 \rangle$ reaching 0.01 level

Separation Power

$$\langle S^2 \rangle = \frac{1}{2} \sum_{i=1}^{n_{\text{bins}}} \frac{(h_{1,i} - h_{2,i})^2}{h_{1,i} + h_{2,i}}$$

[2009.03796]

Arbitrary Generated Shower

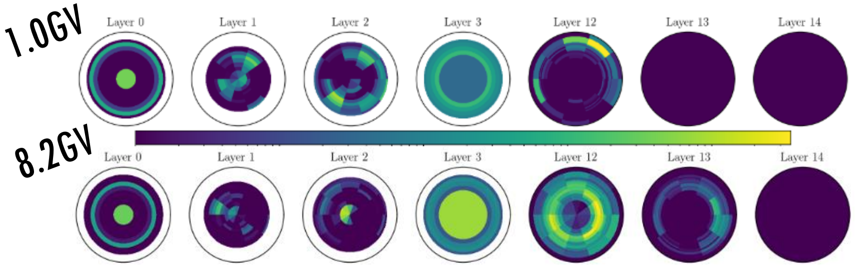


Average Shower

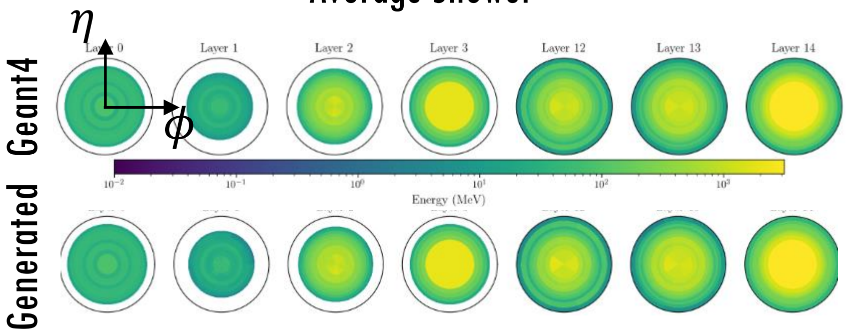


Total Energy Response (ΣE/Ec)

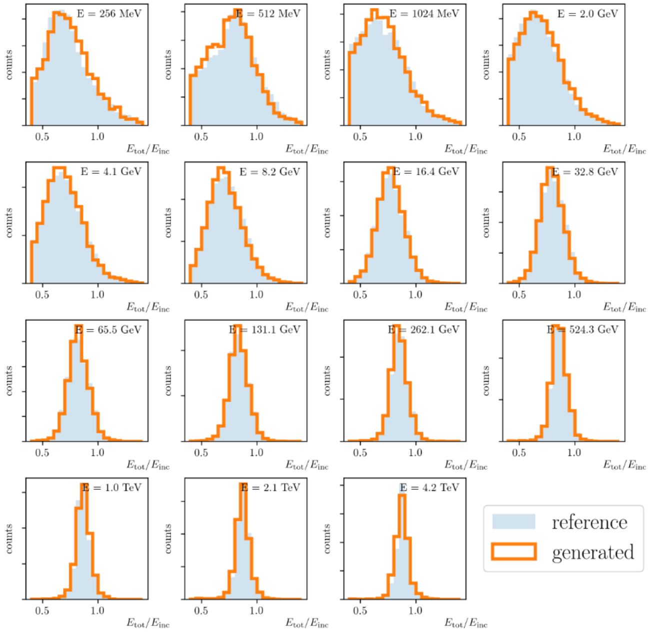


$\langle S^2 \rangle$=0.001~ 0.01

Selections of well-modelled distributions

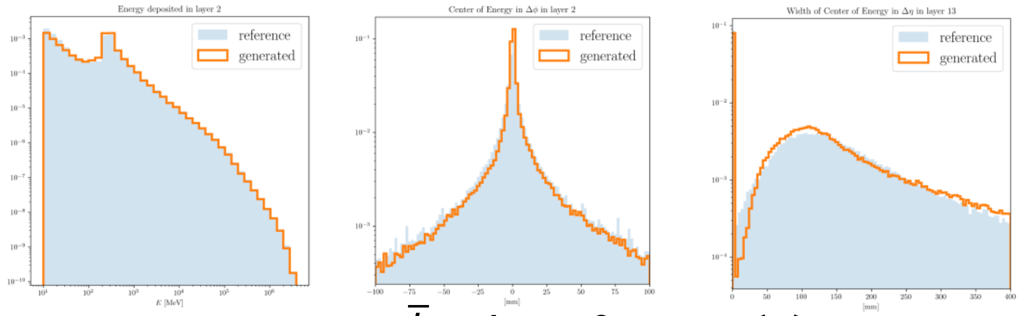


ΣE of layer2 | $\bar{\phi}$ in layer2 | $\sigma(\eta)$ in layer13

| Metrics Per Layer | Mean | Best | Worst |
|---|---|---|---|
| ΣE | 0.003 | 0.001 | 0.006 |
| Shower Center | 0.014 | 0.009 | 0.019 |
| Shower Width | 0.017 | 0.006 | 0.037 |

$\langle S^2 \rangle$ of All Variables

# Scale to Large Dataset

- Orthogonal segmentation: cylindrical convolution operator
- Equivariant down-/up- sampling: FFT resampling
- Residual and Attention: capture of long-range information
- Layer-wise normalization: ΣE layer encoded into latent codes
- Tricks of training: HPO, adaptive weight, … and *patience*

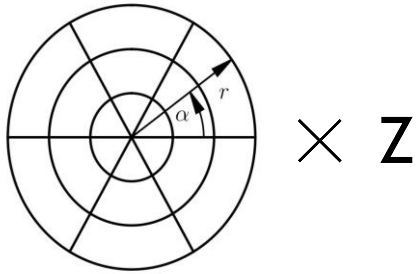


| Datasets | Ch(Z) | Ch(α) | Ch(r) |
|---|---|---|---|
| "Easy" | 5/7 | (Irregular) | |
| **"Medium"** | **45** | **16** | **9** |
| **"Hard"** | **45** | **50** | **18** |

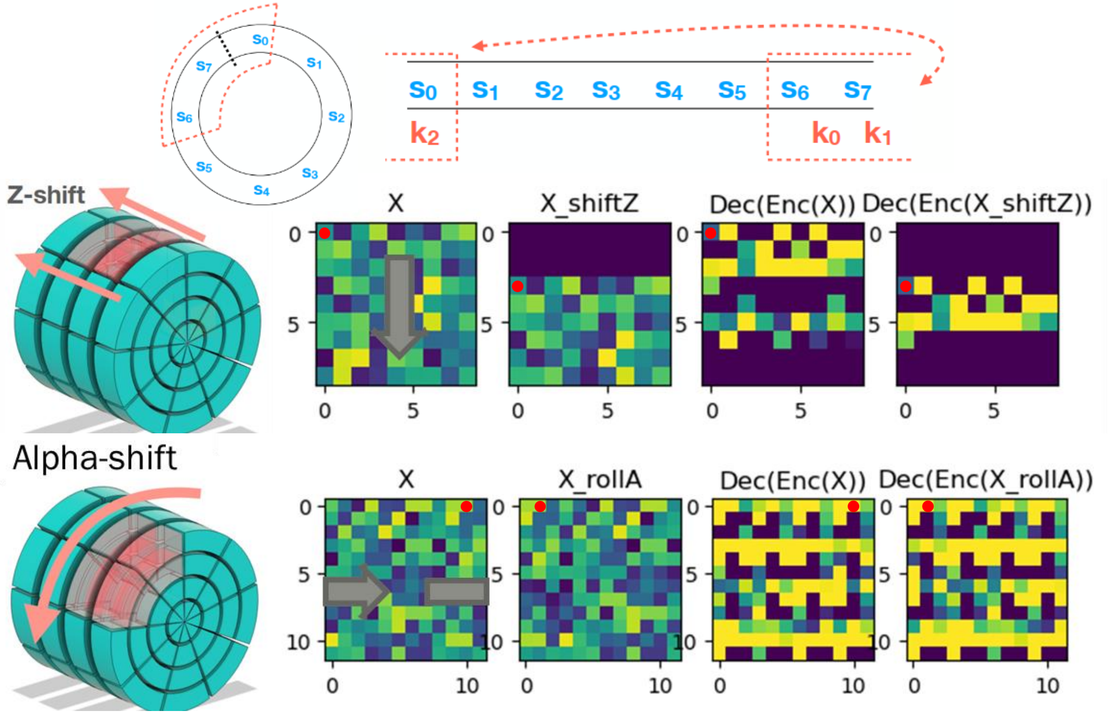


FFT down-sampling

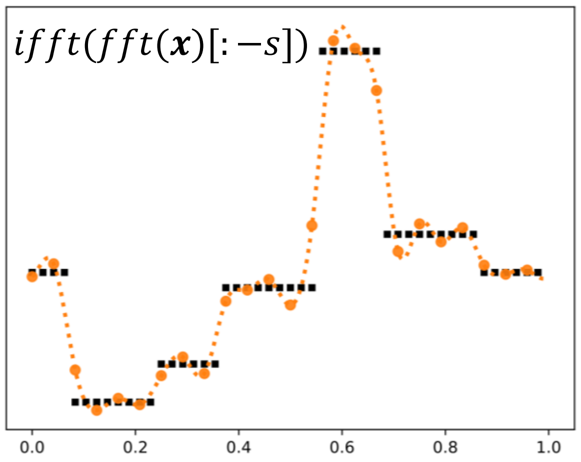


Typical Loss Curve

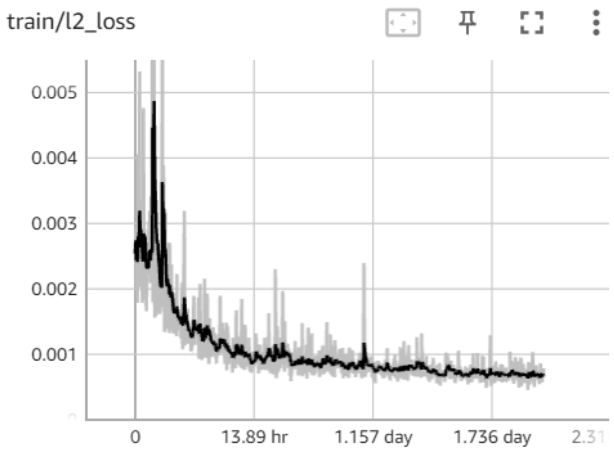

# Scale to Large Dataset

$D = 6480$

Geant4

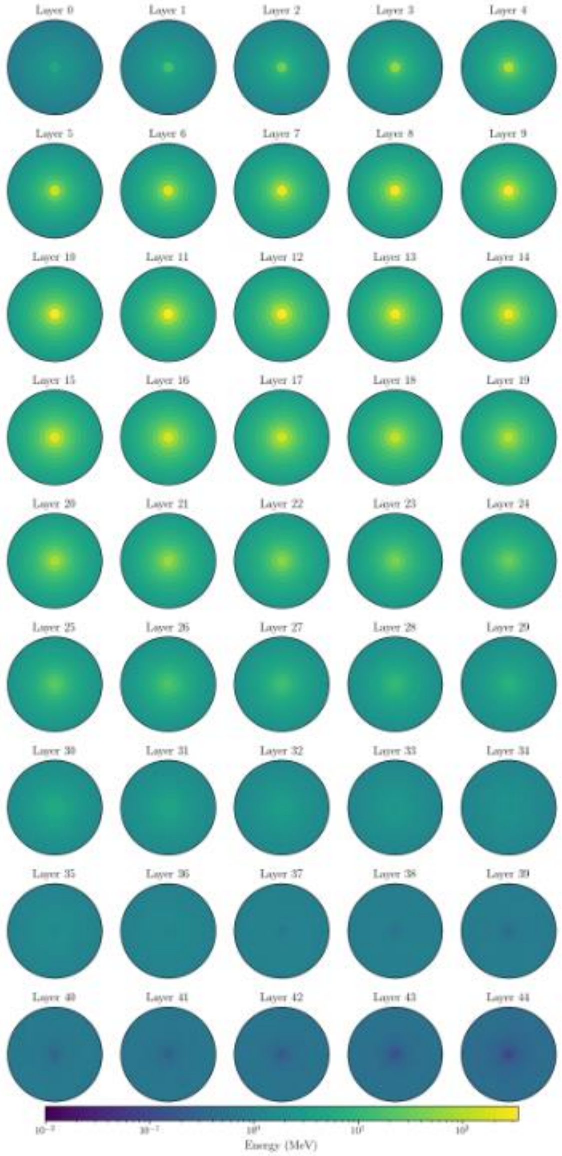


Generated

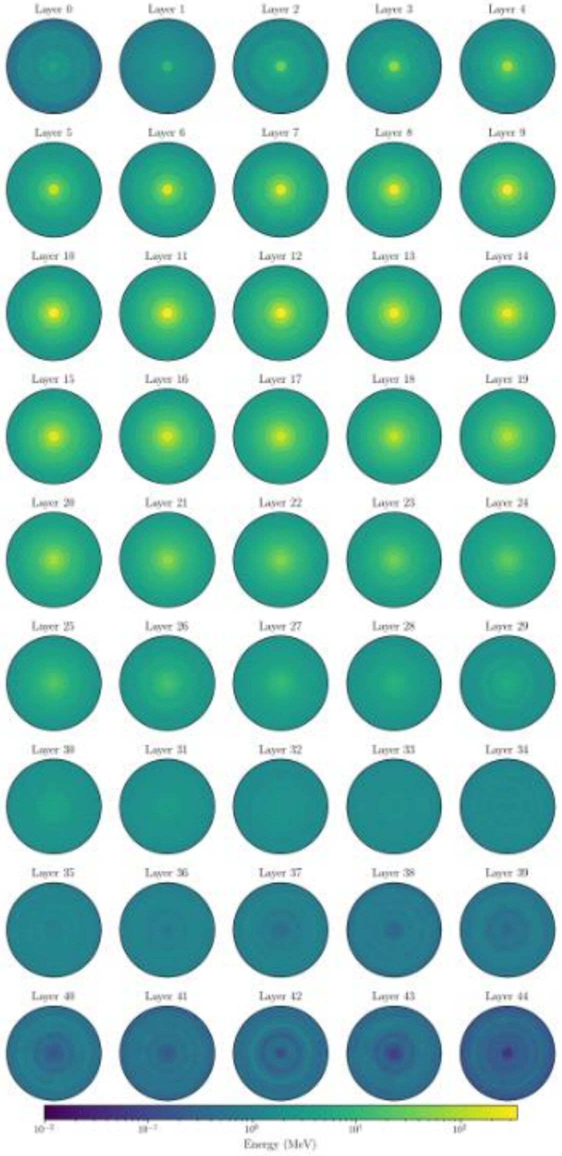


- In general good agreement with input
- Not perfect at first and last several calo. layers

→ Higher sparsity, larger dynamic range, lower stats

## Selections of well-modelled distributions

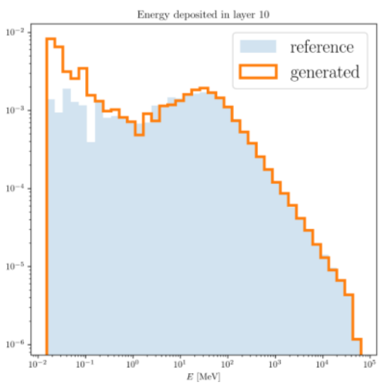


ΣE of layer10

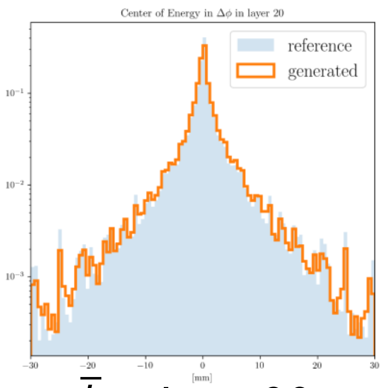


$\bar{\phi}$ in layer20

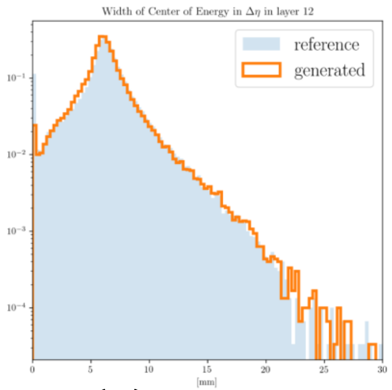


$\sigma(\eta)$ in layer12

| Metrics Per Layer | Mean | Best | Worst |
|---|---|---|---|
| ΣE | 0.009 | 0.001 | 0.024 |
| Shower Center | 0.012 | 0.002 | 0.033 |
| Shower Width | 0.020 | 0.003 | 0.057 |

# Scale to Large Dataset

$D = 40500$

- 2 models with different N#pars. and complexity
- $\langle S^2 \rangle$ reaching 0.01 for energy response and 0.02 for shower shape
- Generally good modelling of inner calo. layers

## Arbitrary Generated Shower (162.28GeV)

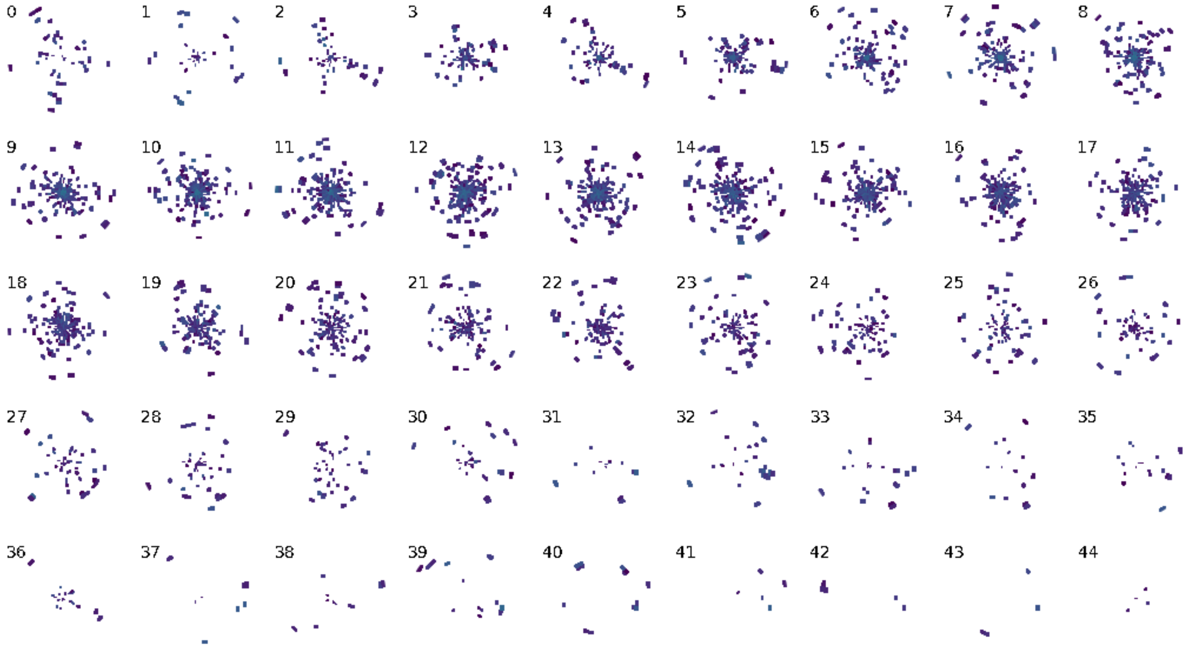


## Distribution at Layer20

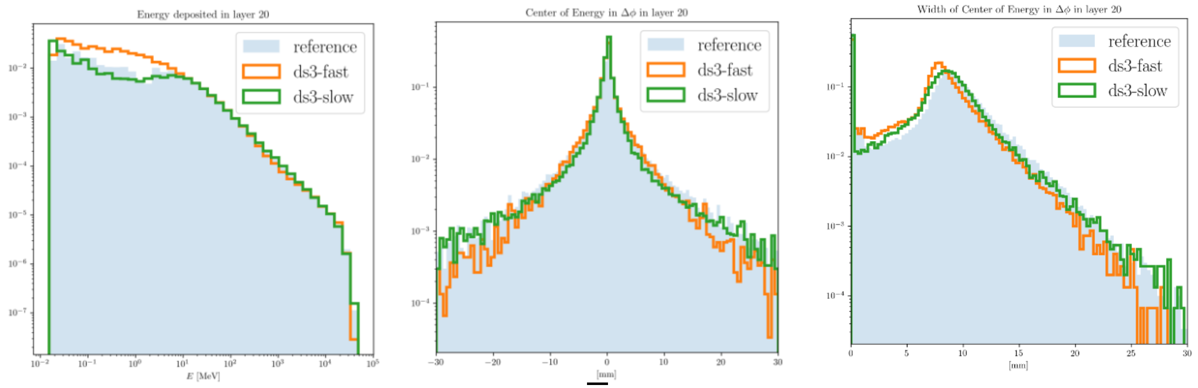


$\Sigma E$ $\bar{\phi}$ $\sigma(\phi)$

| ds3-fast | Mean | Best | Worst |
|---|---|---|---|
| ΣE | 0.021 | 0.002 | 0.130 |
| Shower Center | 0.024 | 0.003 | 0.076 |
| Shower Width | 0.044 | 0.004 | 0.133 |

| ds3-slow | Mean | Best | Worst |
|---|---|---|---|
| ΣE | 0.004 | 0.001 | 0.011 |
| Shower Center | 0.014 | 0.007 | 0.045 |
| Shower Width | 0.032 | 0.006 | 0.095 |

# Performance Summary

- Sampling time tested on1xV100 GPU with 512 showers/batch
- Step1 (en/decoder) forward time at same level regardless of geometry
- Step2 (transformer) dominated for the total sampling time
- $\langle S^2 \rangle$ measured all the energy and shape variables of different calo. layers:
- Best performed layers reach 0.001 and worst at 0.1 level

| Model | Chan. (D) | S1 time/ms | S2 time/ms | Total time/ms | Latent Size (L) | Best $\langle S^2 \rangle$ | Worst $\langle S^2 \rangle$ |
|---|---|---|---|---|---|---|---|
| ds1-photon | 368 | 0.02 | 0.23 | 0.25 | 42 | 0.001 | 0.023 |
| ds1-pion | 533 | 0.02 | 0.26 | 0.28 | 46 | 0.001 | 0.037 |
| ds2 | 6480 | 0.17 | 0.46 | 0.63 | 70 | 0.001 | 0.057 |
| ds3-fast | 40500 | 0.35 | 0.79 | 1.14 | 184 | 0.002 | 0.133 |
| ds3-slow | 40500 | 1.7 | 34.4 | 36.1 | 274 | 0.001 | 0.095 |

# Thinking of VAE model in Calorimeter Fast Simulation

Open for Ideas!

## Promising way to compress the high dimensional calo. data or scale other model:

- However high demanding of engineering effort

## Well-controlled and general latent space:

- Useful for downstream tasks, e.g. reconstruction
- Interplay with foundation model

## Information bottleneck or “limitation”:

- More of less reduced the randomness and shorter “period”
- Higher compression, worse classifier score (easier to be caught)

Various Step1 En/Decoder Models for Dataset3

| Latent size \|L\| | AUC (50k cls-low) |
|---|---|
| 140 | 0.9998 |
| 184 | 0.9962 |
| 274 | 0.9426 |
| 900 | 0.7876 |

## Potential usage of a super-fast latent-labeled simulation model:

- On-the-fly testing of a real-time reconstruction system?
- “Deterministic” fast simulation (like a labeled image)?
- More ideas?

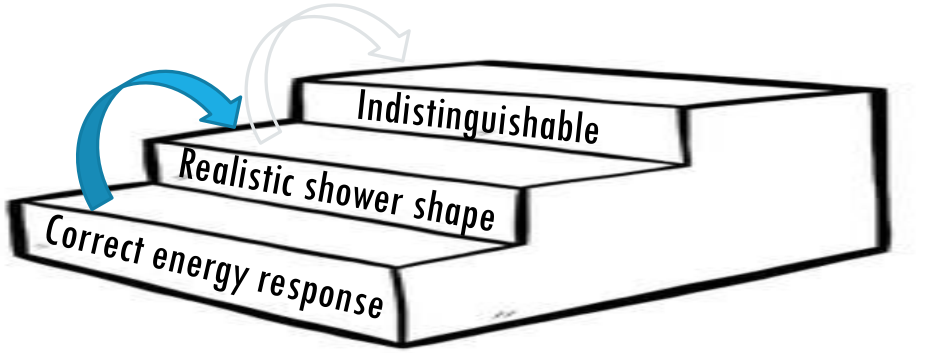

# Concluding

Calorimeter simulation is vital in HEP but computing-intensive

Machine learning methods show great potential for fast-calo-sim

**Two steps model proposed based on VQVAE architecture**

- **Vector Quantization enabling well controlled compression and flexible latent space**
- **GPT model adapted to do the conditional sample in the latent space**

Methods designed for calorimeter data:

- Soft-max normalization, FFT resampling, cylindrical convolution

Performance on CaloChallenge datasets presented

- Promising performance on averaging shower and distribution of key variables
- Ultra-fast generation and scaling dominated by latent model
- Quality of generated detail features not perfect: more study ongoing

Potential application of latent based ultra-fast calo. simulation

# Thanks for your Attention!

# Full Evaluations for Photon Dataset

# Full Evaluations for Pion Dataset

# Full Evaluations for Dataset2

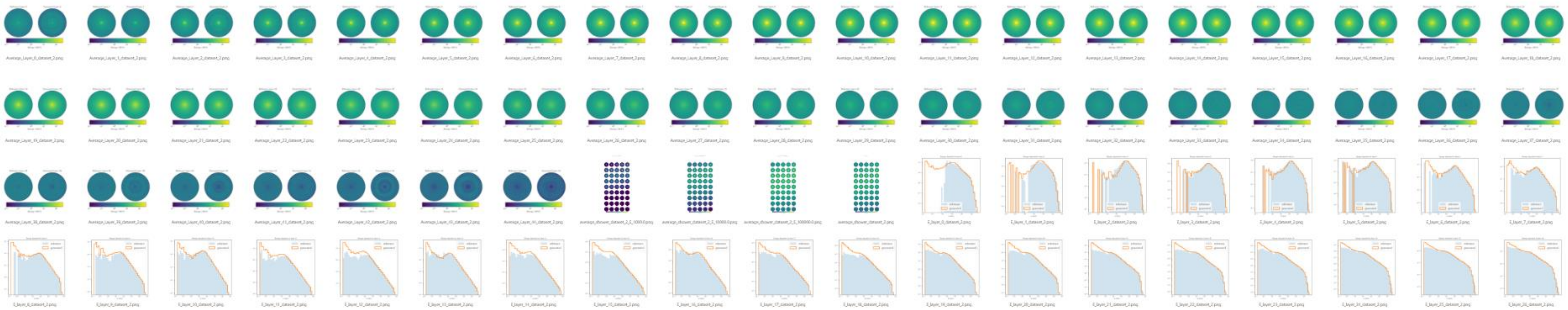

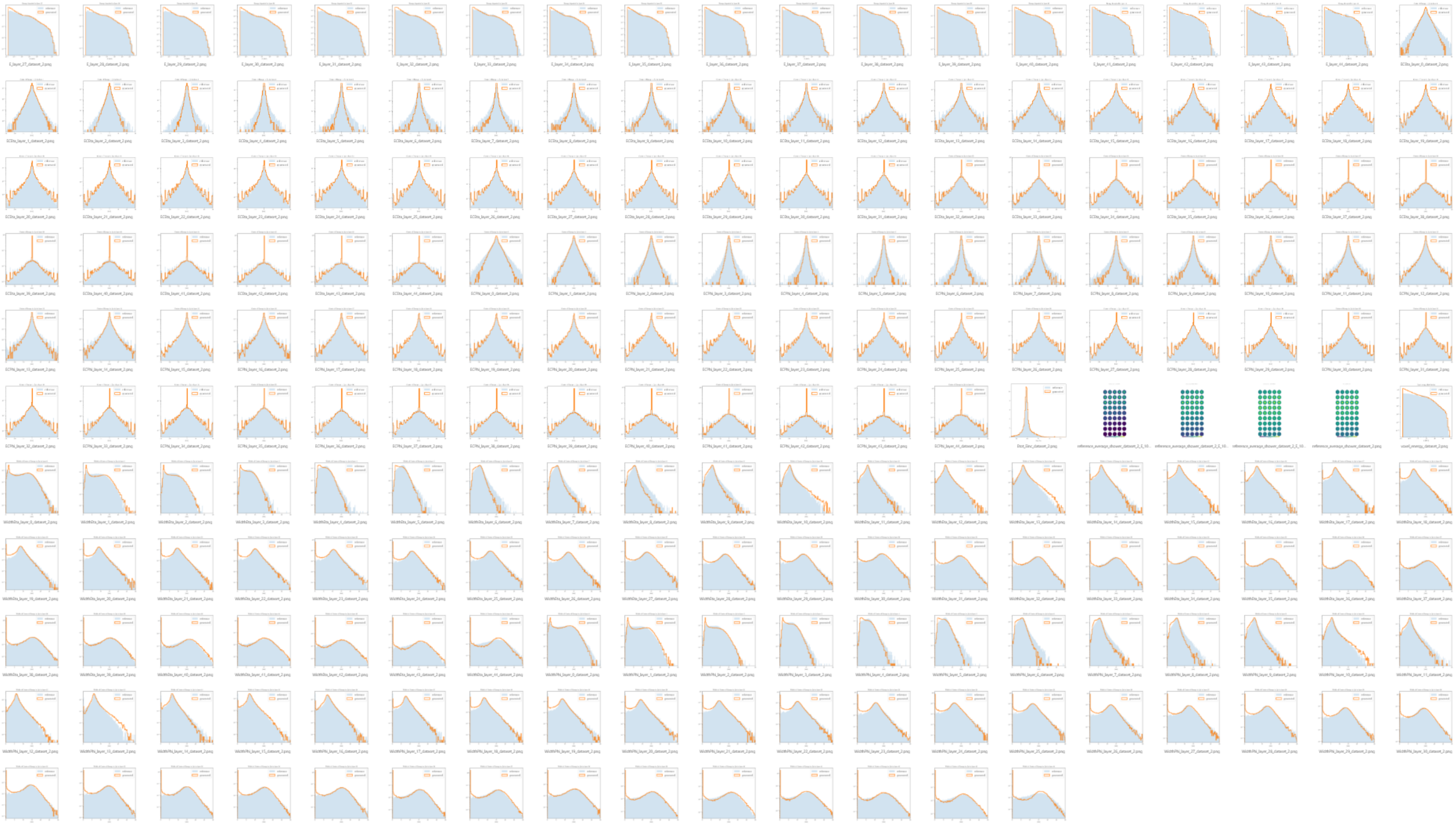

E_layer_27_dataset_2.png E_layer_28_dataset_2.png E_layer_29_dataset_2.png E_layer_30_dataset_2.png E_layer_31_dataset_2.png E_layer_32_dataset_2.png E_layer_33_dataset_2.png E_layer_34_dataset_2.png E_layer_35_dataset_2.png E_layer_36_dataset_2.png E_layer_37_dataset_2.png E_layer_38_dataset_2.png E_layer_39_dataset_2.png E_layer_40_dataset_2.png E_layer_41_dataset_2.png E_layer_42_dataset_2.png E_layer_43_dataset_2.png E_layer_44_dataset_2.png ECEta_layer_0_dataset_2.png

ECEta_layer_1_dataset_2.png ECEta_layer_2_dataset_2.png ECEta_layer_3_dataset_2.png ECEta_layer_4_dataset_2.png ECEta_layer_5_dataset_2.png ECEta_layer_6_dataset_2.png ECEta_layer_7_dataset_2.png ECEta_layer_8_dataset_2.png ECEta_layer_9_dataset_2.png ECEta_layer_10_dataset_2.png ECEta_layer_11_dataset_2.png ECEta_layer_12_dataset_2.png ECEta_layer_13_dataset_2.png ECEta_layer_14_dataset_2.png ECEta_layer_15_dataset_2.png ECEta_layer_16_dataset_2.png ECEta_layer_17_dataset_2.png ECEta_layer_18_dataset_2.png ECEta_layer_19_dataset_2.png

ECEta_layer_20_dataset_2.png ECEta_layer_21_dataset_2.png ECEta_layer_22_dataset_2.png ECEta_layer_23_dataset_2.png ECEta_layer_24_dataset_2.png ECEta_layer_25_dataset_2.png ECEta_layer_26_dataset_2.png ECEta_layer_27_dataset_2.png ECEta_layer_28_dataset_2.png ECEta_layer_29_dataset_2.png ECEta_layer_30_dataset_2.png ECEta_layer_31_dataset_2.png ECEta_layer_32_dataset_2.png ECEta_layer_33_dataset_2.png ECEta_layer_34_dataset_2.png ECEta_layer_35_dataset_2.png ECEta_layer_36_dataset_2.png ECEta_layer_37_dataset_2.png ECEta_layer_38_dataset_2.png

ECEta_layer_39_dataset_2.png ECEta_layer_40_dataset_2.png ECEta_layer_41_dataset_2.png ECEta_layer_42_dataset_2.png ECEta_layer_43_dataset_2.png ECEta_layer_44_dataset_2.png ECPhi_layer_0_dataset_2.png ECPhi_layer_1_dataset_2.png ECPhi_layer_2_dataset_2.png ECPhi_layer_3_dataset_2.png ECPhi_layer_4_dataset_2.png ECPhi_layer_5_dataset_2.png ECPhi_layer_6_dataset_2.png ECPhi_layer_7_dataset_2.png ECPhi_layer_8_dataset_2.png ECPhi_layer_9_dataset_2.png ECPhi_layer_10_dataset_2.png ECPhi_layer_11_dataset_2.png ECPhi_layer_12_dataset_2.png

ECPhi_layer_13_dataset_2.png ECPhi_layer_14_dataset_2.png ECPhi_layer_15_dataset_2.png ECPhi_layer_16_dataset_2.png ECPhi_layer_17_dataset_2.png ECPhi_layer_18_dataset_2.png ECPhi_layer_19_dataset_2.png ECPhi_layer_20_dataset_2.png ECPhi_layer_21_dataset_2.png ECPhi_layer_22_dataset_2.png ECPhi_layer_23_dataset_2.png ECPhi_layer_24_dataset_2.png ECPhi_layer_25_dataset_2.png ECPhi_layer_26_dataset_2.png ECPhi_layer_27_dataset_2.png ECPhi_layer_28_dataset_2.png ECPhi_layer_29_dataset_2.png ECPhi_layer_30_dataset_2.png ECPhi_layer_31_dataset_2.png

ECPhi_layer_32_dataset_2.png ECPhi_layer_33_dataset_2.png ECPhi_layer_34_dataset_2.png ECPhi_layer_35_dataset_2.png ECPhi_layer_36_dataset_2.png ECPhi_layer_37_dataset_2.png ECPhi_layer_38_dataset_2.png ECPhi_layer_39_dataset_2.png ECPhi_layer_40_dataset_2.png ECPhi_layer_41_dataset_2.png ECPhi_layer_42_dataset_2.png ECPhi_layer_43_dataset_2.png ECPhi_layer_44_dataset_2.png Etot_Einc_dataset_2.png reference_average_shower_dataset_2_E_10... reference_average_shower_dataset_2_E_10... reference_average_shower_dataset_2_E_10... reference_average_shower_dataset_2.png voxel_energy_dataset_2.png

WidthEta_layer_0_dataset_2.png WidthEta_layer_1_dataset_2.png WidthEta_layer_2_dataset_2.png WidthEta_layer_3_dataset_2.png WidthEta_layer_4_dataset_2.png WidthEta_layer_5_dataset_2.png WidthEta_layer_6_dataset_2.png WidthEta_layer_7_dataset_2.png WidthEta_layer_8_dataset_2.png WidthEta_layer_9_dataset_2.png WidthEta_layer_10_dataset_2.png WidthEta_layer_11_dataset_2.png WidthEta_layer_12_dataset_2.png WidthEta_layer_13_dataset_2.png WidthEta_layer_14_dataset_2.png WidthEta_layer_15_dataset_2.png WidthEta_layer_16_dataset_2.png WidthEta_layer_17_dataset_2.png WidthEta_layer_18_dataset_2.png

WidthEta_layer_19_dataset_2.png WidthEta_layer_20_dataset_2.png WidthEta_layer_21_dataset_2.png WidthEta_layer_22_dataset_2.png WidthEta_layer_23_dataset_2.png WidthEta_layer_24_dataset_2.png WidthEta_layer_25_dataset_2.png WidthEta_layer_26_dataset_2.png WidthEta_layer_27_dataset_2.png WidthEta_layer_28_dataset_2.png WidthEta_layer_29_dataset_2.png WidthEta_layer_30_dataset_2.png WidthEta_layer_31_dataset_2.png WidthEta_layer_32_dataset_2.png WidthEta_layer_33_dataset_2.png WidthEta_layer_34_dataset_2.png WidthEta_layer_35_dataset_2.png WidthEta_layer_36_dataset_2.png WidthEta_layer_37_dataset_2.png

WidthEta_layer_38_dataset_2.png WidthEta_layer_39_dataset_2.png WidthEta_layer_40_dataset_2.png WidthEta_layer_41_dataset_2.png WidthEta_layer_42_dataset_2.png WidthEta_layer_43_dataset_2.png WidthEta_layer_44_dataset_2.png WidthPhi_layer_0_dataset_2.png WidthPhi_layer_1_dataset_2.png WidthPhi_layer_2_dataset_2.png WidthPhi_layer_3_dataset_2.png WidthPhi_layer_4_dataset_2.png WidthPhi_layer_5_dataset_2.png WidthPhi_layer_6_dataset_2.png WidthPhi_layer_7_dataset_2.png WidthPhi_layer_8_dataset_2.png WidthPhi_layer_9_dataset_2.png WidthPhi_layer_10_dataset_2.png WidthPhi_layer_11_dataset_2.png

WidthPhi_layer_12_dataset_2.png WidthPhi_layer_13_dataset_2.png WidthPhi_layer_14_dataset_2.png WidthPhi_layer_15_dataset_2.png WidthPhi_layer_16_dataset_2.png WidthPhi_layer_17_dataset_2.png WidthPhi_layer_18_dataset_2.png WidthPhi_layer_19_dataset_2.png WidthPhi_layer_20_dataset_2.png WidthPhi_layer_21_dataset_2.png WidthPhi_layer_22_dataset_2.png WidthPhi_layer_23_dataset_2.png WidthPhi_layer_24_dataset_2.png WidthPhi_layer_25_dataset_2.png WidthPhi_layer_26_dataset_2.png WidthPhi_layer_27_dataset_2.png WidthPhi_layer_28_dataset_2.png WidthPhi_layer_29_dataset_2.png WidthPhi_layer_30_dataset_2.png

WidthPhi_layer_31_dataset_2.png WidthPhi_layer_32_dataset_2.png WidthPhi_layer_33_dataset_2.png WidthPhi_layer_34_dataset_2.png WidthPhi_layer_35_dataset_2.png WidthPhi_layer_36_dataset_2.png WidthPhi_layer_37_dataset_2.png WidthPhi_layer_38_dataset_2.png WidthPhi_layer_39_dataset_2.png WidthPhi_layer_40_dataset_2.png WidthPhi_layer_41_dataset_2.png WidthPhi_layer_42_dataset_2.png WidthPhi_layer_43_dataset_2.png WidthPhi_layer_44_dataset_2.png

# Full Evaluations for Dataset3 (slow model)

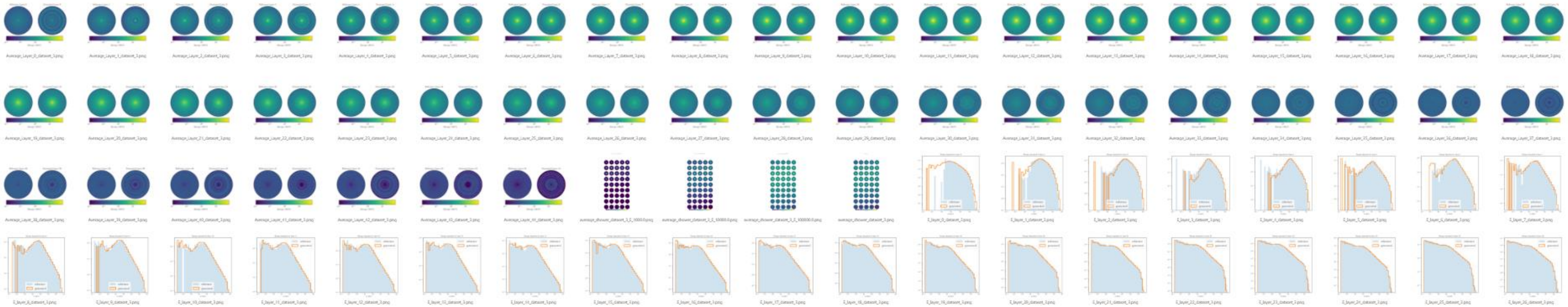

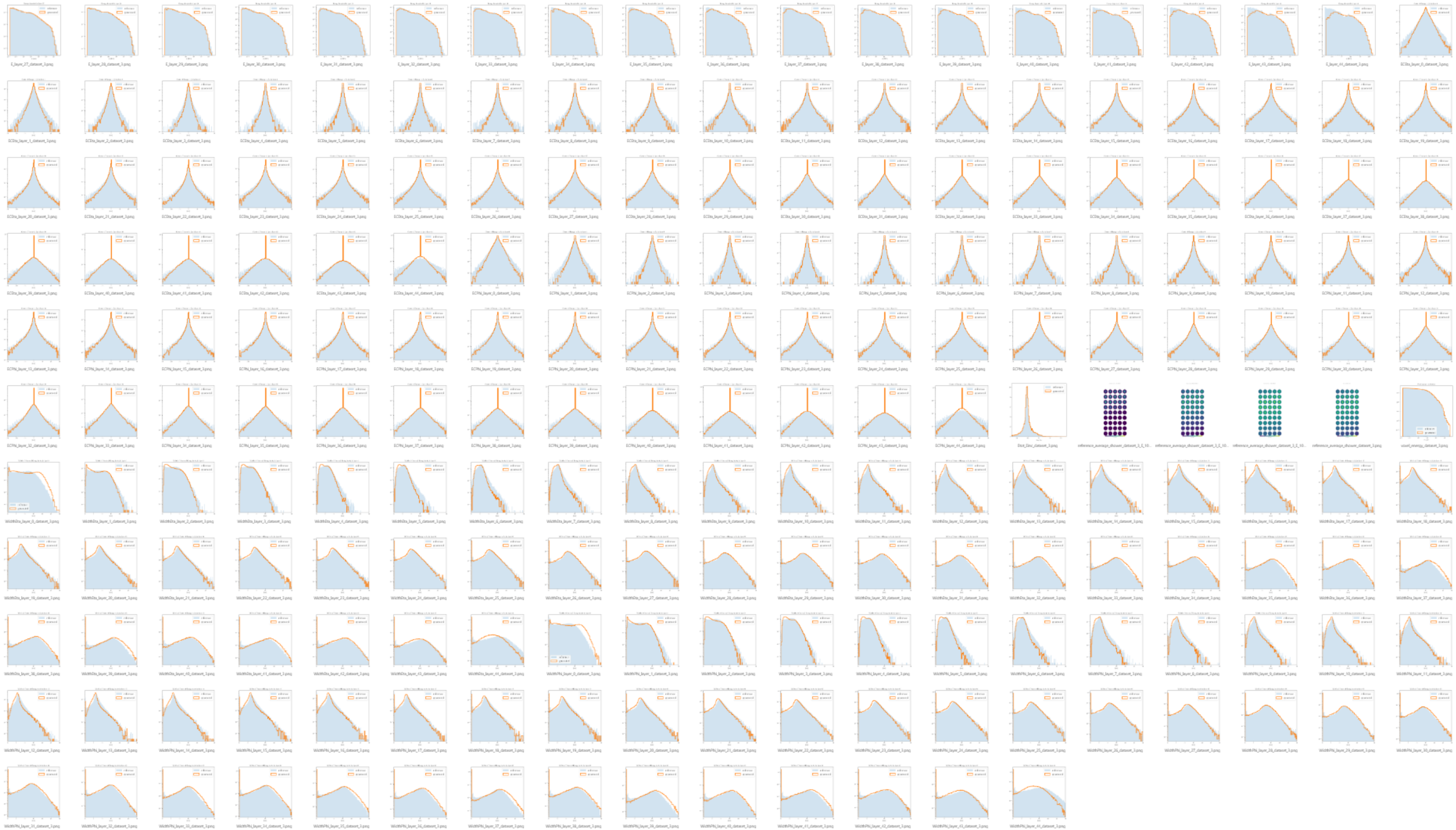

E_layer_27_dataset_3.png
E_layer_28_dataset_3.png
E_layer_29_dataset_3.png
E_layer_30_dataset_3.png
E_layer_31_dataset_3.png
E_layer_32_dataset_3.png
E_layer_33_dataset_3.png
E_layer_34_dataset_3.png
E_layer_35_dataset_3.png
E_layer_36_dataset_3.png
E_layer_37_dataset_3.png
E_layer_38_dataset_3.png
E_layer_39_dataset_3.png
E_layer_40_dataset_3.png
E_layer_41_dataset_3.png
E_layer_42_dataset_3.png
E_layer_43_dataset_3.png
E_layer_44_dataset_3.png
ECEta_layer_0_dataset_3.png
ECEta_layer_1_dataset_3.png
ECEta_layer_2_dataset_3.png
ECEta_layer_3_dataset_3.png
ECEta_layer_4_dataset_3.png
ECEta_layer_5_dataset_3.png
ECEta_layer_6_dataset_3.png
ECEta_layer_7_dataset_3.png
ECEta_layer_8_dataset_3.png
ECEta_layer_9_dataset_3.png
ECEta_layer_10_dataset_3.png
ECEta_layer_11_dataset_3.png
ECEta_layer_12_dataset_3.png
ECEta_layer_13_dataset_3.png
ECEta_layer_14_dataset_3.png
ECEta_layer_15_dataset_3.png
ECEta_layer_16_dataset_3.png
ECEta_layer_17_dataset_3.png
ECEta_layer_18_dataset_3.png
ECEta_layer_19_dataset_3.png
ECEta_layer_20_dataset_3.png
ECEta_layer_21_dataset_3.png
ECEta_layer_22_dataset_3.png
ECEta_layer_23_dataset_3.png
ECEta_layer_24_dataset_3.png
ECEta_layer_25_dataset_3.png
ECEta_layer_26_dataset_3.png
ECEta_layer_27_dataset_3.png
ECEta_layer_28_dataset_3.png
ECEta_layer_29_dataset_3.png
ECEta_layer_30_dataset_3.png
ECEta_layer_31_dataset_3.png
ECEta_layer_32_dataset_3.png
ECEta_layer_33_dataset_3.png
ECEta_layer_34_dataset_3.png
ECEta_layer_35_dataset_3.png
ECEta_layer_36_dataset_3.png
ECEta_layer_37_dataset_3.png
ECEta_layer_38_dataset_3.png
ECEta_layer_39_dataset_3.png
ECEta_layer_40_dataset_3.png
ECEta_layer_41_dataset_3.png
ECEta_layer_42_dataset_3.png
ECEta_layer_43_dataset_3.png
ECEta_layer_44_dataset_3.png
ECPhi_layer_0_dataset_3.png
ECPhi_layer_1_dataset_3.png
ECPhi_layer_2_dataset_3.png
ECPhi_layer_3_dataset_3.png
ECPhi_layer_4_dataset_3.png
ECPhi_layer_5_dataset_3.png
ECPhi_layer_6_dataset_3.png
ECPhi_layer_7_dataset_3.png
ECPhi_layer_8_dataset_3.png
ECPhi_layer_9_dataset_3.png
ECPhi_layer_10_dataset_3.png
ECPhi_layer_11_dataset_3.png
ECPhi_layer_12_dataset_3.png
ECPhi_layer_13_dataset_3.png
ECPhi_layer_14_dataset_3.png
ECPhi_layer_15_dataset_3.png
ECPhi_layer_16_dataset_3.png
ECPhi_layer_17_dataset_3.png
ECPhi_layer_18_dataset_3.png
ECPhi_layer_19_dataset_3.png
ECPhi_layer_20_dataset_3.png
ECPhi_layer_21_dataset_3.png
ECPhi_layer_22_dataset_3.png
ECPhi_layer_23_dataset_3.png
ECPhi_layer_24_dataset_3.png
ECPhi_layer_25_dataset_3.png
ECPhi_layer_26_dataset_3.png
ECPhi_layer_27_dataset_3.png
ECPhi_layer_28_dataset_3.png
ECPhi_layer_29_dataset_3.png
ECPhi_layer_30_dataset_3.png
ECPhi_layer_31_dataset_3.png
ECPhi_layer_32_dataset_3.png
ECPhi_layer_33_dataset_3.png
ECPhi_layer_34_dataset_3.png
ECPhi_layer_35_dataset_3.png
ECPhi_layer_36_dataset_3.png
ECPhi_layer_37_dataset_3.png
ECPhi_layer_38_dataset_3.png
ECPhi_layer_39_dataset_3.png
ECPhi_layer_40_dataset_3.png
ECPhi_layer_41_dataset_3.png
ECPhi_layer_42_dataset_3.png
ECPhi_layer_43_dataset_3.png
ECPhi_layer_44_dataset_3.png
Etot_Einc_dataset_3.png
reference_average_shower_dataset_3_E_10...
reference_average_shower_dataset_3_E_10...
reference_average_shower_dataset_3_E_10...
reference_average_shower_dataset_3.png
voxel_energy_dataset_3.png
WidthEta_layer_0_dataset_3.png
WidthEta_layer_1_dataset_3.png
WidthEta_layer_2_dataset_3.png
WidthEta_layer_3_dataset_3.png
WidthEta_layer_4_dataset_3.png
WidthEta_layer_5_dataset_3.png
WidthEta_layer_6_dataset_3.png
WidthEta_layer_7_dataset_3.png
WidthEta_layer_8_dataset_3.png
WidthEta_layer_9_dataset_3.png
WidthEta_layer_10_dataset_3.png
WidthEta_layer_11_dataset_3.png
WidthEta_layer_12_dataset_3.png
WidthEta_layer_13_dataset_3.png
WidthEta_layer_14_dataset_3.png
WidthEta_layer_15_dataset_3.png
WidthEta_layer_16_dataset_3.png
WidthEta_layer_17_dataset_3.png
WidthEta_layer_18_dataset_3.png
WidthEta_layer_19_dataset_3.png
WidthEta_layer_20_dataset_3.png
WidthEta_layer_21_dataset_3.png
WidthEta_layer_22_dataset_3.png
WidthEta_layer_23_dataset_3.png
WidthEta_layer_24_dataset_3.png
WidthEta_layer_25_dataset_3.png
WidthEta_layer_26_dataset_3.png
WidthEta_layer_27_dataset_3.png
WidthEta_layer_28_dataset_3.png
WidthEta_layer_29_dataset_3.png
WidthEta_layer_30_dataset_3.png
WidthEta_layer_31_dataset_3.png
WidthEta_layer_32_dataset_3.png
WidthEta_layer_33_dataset_3.png
WidthEta_layer_34_dataset_3.png
WidthEta_layer_35_dataset_3.png
WidthEta_layer_36_dataset_3.png
WidthEta_layer_37_dataset_3.png
WidthEta_layer_38_dataset_3.png
WidthEta_layer_39_dataset_3.png
WidthEta_layer_40_dataset_3.png
WidthEta_layer_41_dataset_3.png
WidthEta_layer_42_dataset_3.png
WidthEta_layer_43_dataset_3.png
WidthEta_layer_44_dataset_3.png
WidthPhi_layer_0_dataset_3.png
WidthPhi_layer_1_dataset_3.png
WidthPhi_layer_2_dataset_3.png
WidthPhi_layer_3_dataset_3.png
WidthPhi_layer_4_dataset_3.png
WidthPhi_layer_5_dataset_3.png
WidthPhi_layer_6_dataset_3.png
WidthPhi_layer_7_dataset_3.png
WidthPhi_layer_8_dataset_3.png
WidthPhi_layer_9_dataset_3.png
WidthPhi_layer_10_dataset_3.png
WidthPhi_layer_11_dataset_3.png
WidthPhi_layer_12_dataset_3.png
WidthPhi_layer_13_dataset_3.png
WidthPhi_layer_14_dataset_3.png
WidthPhi_layer_15_dataset_3.png
WidthPhi_layer_16_dataset_3.png
WidthPhi_layer_17_dataset_3.png
WidthPhi_layer_18_dataset_3.png
WidthPhi_layer_19_dataset_3.png
WidthPhi_layer_20_dataset_3.png
WidthPhi_layer_21_dataset_3.png
WidthPhi_layer_22_dataset_3.png
WidthPhi_layer_23_dataset_3.png
WidthPhi_layer_24_dataset_3.png
WidthPhi_layer_25_dataset_3.png
WidthPhi_layer_26_dataset_3.png
WidthPhi_layer_27_dataset_3.png
WidthPhi_layer_28_dataset_3.png
WidthPhi_layer_29_dataset_3.png
WidthPhi_layer_30_dataset_3.png
WidthPhi_layer_31_dataset_3.png
WidthPhi_layer_32_dataset_3.png
WidthPhi_layer_33_dataset_3.png
WidthPhi_layer_34_dataset_3.png
WidthPhi_layer_35_dataset_3.png
WidthPhi_layer_36_dataset_3.png
WidthPhi_layer_37_dataset_3.png
WidthPhi_layer_38_dataset_3.png
WidthPhi_layer_39_dataset_3.png
WidthPhi_layer_40_dataset_3.png
WidthPhi_layer_41_dataset_3.png
WidthPhi_layer_42_dataset_3.png
WidthPhi_layer_43_dataset_3.png
WidthPhi_layer_44_dataset_3.png